13th Australia New Zealand Conference on Geomechanics – Acosta-Martínez & Lehane (Eds.)

Estimating the drained friction capacity of pipelines on mobile seabeds

J.G. Tom & T.J. Griffiths
Centre for Offshore Foundation Systems, University of Western Australia, Perth, Australia

D.J. White
University of Southampton, Southampton, United Kingdom (and UWA)

S.H.F. Leckie
GHD, Perth, Australia

ABSTRACT: Pipelines resting on mobile sandy seabeds must be adequately stable under hydrodynamic action. This paper describes numerical analyses to establish the available geotechnical capacity – defined via generalised drained failure envelopes – of pipelines placed on seabeds subject to sediment mobility. Seabed mobility often causes an upward or downward-sloping profile of ground adjacent to the pipe, which has a strong influence on the stability, in combination with the embedment depth. Finite element limit analyses are conducted to assess the peak lateral breakout resistance for a seabed that is idealised as a cohesionless Mohr-Coulomb material. A wide range of combinations of embedment and sloping profile are analysed. The accuracy of two simple analytical models for the limiting lateral friction are evaluated.

1 INTRODUCTION

1.1 *Subsea pipeline stability and buckling*

Subsea pipelines and cables are commonly used to transport hydrocarbons, power or information across seabeds that are potentially mobile during operational environmental conditions (i.e. tides, storms, etc.). Pipelines laid on mobile seabeds are subject to significant post-lay changes to their embedment. These changes have traditionally been poorly understood in pipeline design practise, and hence either ignored or accounted for in a manner that can be overly conservative (Griffiths et al. 2018; Bransby et al. 2014).

The resulting uncertainty can for example result in the use of additional concrete weight coating to ensure on-bottom stability design under minimal as-laid embedment or require the placement of excessive buckle initiation devices to account for the uncertainty in managing thermal expansion on mobile seabeds. For more reliable and cost-effective pipeline and cable design, it is necessary to understand the through-life embedment, and the resulting stability.

1.2 *Embedment due to sediment mobility*

Recent work has highlighted the influence of seabed mobility in changing the embedment condition of on-bottom pipelines. Interpretation of field observations by Leckie et al. (2015, 2016, 2018) has quantified the post lay embedment changes for a range of pipelines on Australia's North West Shelf. For instance, Leckie et al. (2015) illustrated post-lay changes characterised by intermittent spanning and embedded sections, with the embedment change driven by scour-induced sagging and sinking at span shoulders. Meanwhile, Leckie et al. (2016) illustrated post-lay changes for two parallel flowlines, where the mobility-induced change was driven by sedimentation, which led to the progressive build up of triangular sediment wedges immediately either side of the pipeline (see Figure 1).

Design methods to rigorously account for the resulting lateral resistance following changes in embedment are required to properly capture the increased stability. Generalised solutions can then be applied both in design of new pipelines, and in integrity management of existing facilities.

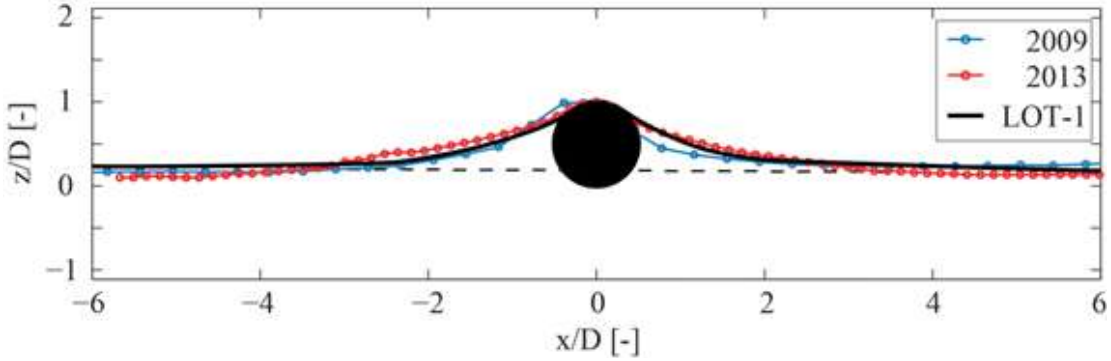

Figure 1. Typical equilibrium seabed profiles following scour and sedimentation reproduced from Leckie et al. (2016). Horizontal dashed line indicates initial seabed.

For example, they can be used to model existing pipelines under adverse loading conditions (see Leckie et al. 2018 for instance), to envelope the future performance of new facilities during their design, or to provide improved understanding of post-operational long-term behaviour. In both cases, statistical analysis and an understanding of the metocean environment allow reliability-based forecasts of the future scour and stability behaviour to be made (e.g. following the methodology set out by Tom et al. 2016 for scour around seabed foundations).

Changes in the embedment geometry cause changes in the resistance provided by the seabed against pipeline lateral, vertical and axial movement. The level of local embedment has a first order impact on the required load to laterally move a pipeline, since with increased embedment more soil must be mobilised and displaced in order for the pipeline to 'breakout' of its position (e.g. Verley & Sotberg, 1994; Martin & White, 2012). However, previous studies (e.g. Bransby et al., 2014; Tom et al., 2015) have shown that the geometrical profile of the seabed sloping away from the pipeline also has a significant influence on the pipeline breakout resistance.

These changes to the seabed resistance associated with local variations in pipeline embedment have impacts on pipeline stability (Griffiths et al. 2018, Draper et al. 2018) as well as thermal buckling management (Westgate et al. 2016), and therefore form a key variable in the design of pipelines in regions with potentially mobile seabeds.

1.3 *Geotechnical idealization for stability analysis*

The current work builds upon previous studies that explored changes in pipe-seabed resistance due to geometry changes through a parametric study over a wider range of geometries. This study is conducted assuming drained shearing conditions at breakout (representative of the sandy sediments that predominate at many mobile sites) using limit analysis.

Drained conditions occur where the rate of loading, or the rate of movement, are sufficiently slow that excess pore pressures are not created. These conditions can be defined by either a dimensionless time of loading, $T = c_v t/D^2$, or a dimensionless velocity of movement, $V = vD/c_v$. In these relationships, D denotes the pipeline diameter and c_v is the coefficient of consolidation. For fully drained conditions, $T >\sim 0.3$ or $V \sim< 0.1$ based on numerical solutions presented by Gourvenec & White (2010) and Chatterjee et al. (2013). For a 0.5m diameter pipeline and a silty soil with a c_v of 1000 m^2/year these limits correspond to a time of 40 minutes or a velocity of 23 mm/hour. For a sandy soil with a typical c_v of 100,000 m^2/year, the limits are 24 seconds and 0.6 mm/s respectively.

Instead of focusing on specific geometries defined based on pipeline surveys, the current study systematically explores the changing capacity for a simple range of idealised embedment profiles. These profiles are defined by two parameters: the local pipeline embedment (e) and the local seabed slope away from the pipeline (θ), as illustrated on Figure 2. The local pipeline embedment is varied from 10% to 90% of the pipeline diameter and seabed slopes of -20° to +20° are considered, which are believed to cover the majority of the range of geometries that may be encountered in practice.

1.4 *Effect of embedment on hydrodynamic loading*

Changes to local embedment and local seabed slope also have a significant effect on the local hydrodynamic forces, especially the resolved inclination of the net force due to lift, drag and submerged weight (e.g. Griffiths 2012; Tong 2016). These changes therefore alter the inclination of pipe loading at failure, including vertical breakout as observed by Cornett et al. (2015). In the present analysis, the loading path adopted in the analysis involves purely horizontal loading, with lift being ignored. To apply the results to a case with lift and drag, in which the V-H load path is known, it may be useful to replot the present results in terms of V and H, rather than friction (H/V) and V.

2 NUMERICAL ANALYSIS METHOD

The analyses in this paper were performed using OptumG2 (OptumCE 2018), which is a commercially available finite element limit analysis (FELA) software. Limit analyses were conducted using the methods outlined by Lyamin and Sloan (2002), incorporating adaptive remeshing to locally optimise the mesh around the failure mechanism of interest (Lyamin et al., 2004). An example refined mesh is shown on Figure 2, which also defines the pertinent problem variables. For this study, the final number of elements used in each analysis was ~5,000. The mesh was spatially refined with an increasing number of elements over 4 steps from 500 initial elements.

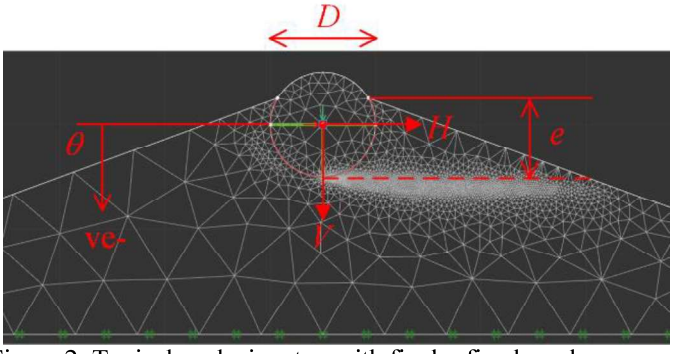

Figure 2. Typical analysis setup with final refined mesh.

The soil in these analyses is assumed to be rigid-plastic following a Mohr-Coloumb failure criteria,

where the cohesion $c = 0$. Limit analysis assumes associated flow and hence the dilation and friction angles are equal. Throughout, a friction angle, ϕ, of 35°, a soil effective unit weight, γ'_s of 7 kN/m^3 and a pipeline diameter, D, of 1 m have been assumed. All results are presented non-dimensionally such that the particular selected values of D and γ'_s are irrelevant. Tom & White (2019) show the effect of relative density and non-associated flow can be captured for relatively small vertical load scenarios through the use of associated flow in combination with a reduced friction angle following Davis (1968).

3 RESULTS

The analyses presented below are generally developed with non-dimensional quantities, where the vertical or horizontal loads are normalised as per (with a similar form for horizontal load):

$$\bar{V} = \frac{V}{D^2 \gamma'_s} \quad (1)$$

where V is the pipe-seabed force per unit length of pipeline (kN/m), D is the pipeline diameter (m) and γ'_s is the soil effective unit weight (kN/m^3). To provide a comparison between this quantity and commonly used terms for pipeline unit weight, Figure 3 compares constant values of $\bar{V}$ with equivalent values of pipeline specific gravity ($SG = \gamma'_p/\gamma_w$) for a range of γ'_s. Common values of effective unit weight are in the range 4 – 10 kN/m^3. Typical values of operating pipeline SG, range from 1.2 for a large diameter gas pipeline to ~3 for umbilicals or cables, with small diameter flowlines lying in between these values. For these conditions, the effective range of $\bar{V}$ is up to about 3. Representative ranges of $\bar{V}$ are higher if the effective unit weight of the soil is small or if the operative ('average') vertical pipe-seabed contact force is elevated above the self-weight due to intermittent spanning (e.g. Leckie et al. 2015, 2016). For most design scenarios under normal operating conditions and typical soil properties, a typical range of $\bar{V}$ would be expected to be less than 3 as considered herein.

All results are presented in terms of the horizontal force at failure for a given vertical load. This may be viewed as the vertical load at the moment of failure, whether reached via a load path of constant or reducing (i.e. lift) vertical load during breakout. For the former, the vertical load is analogous to the self-weight of the pipeline (enhanced, if appropriate, by spanning) if any lift or downforce components that occur during the breakout process are neglected. Hence, in a 2D sense, this means that the pipe is free to move vertically to conform with the required mechanism kinematics at the moment of failure.

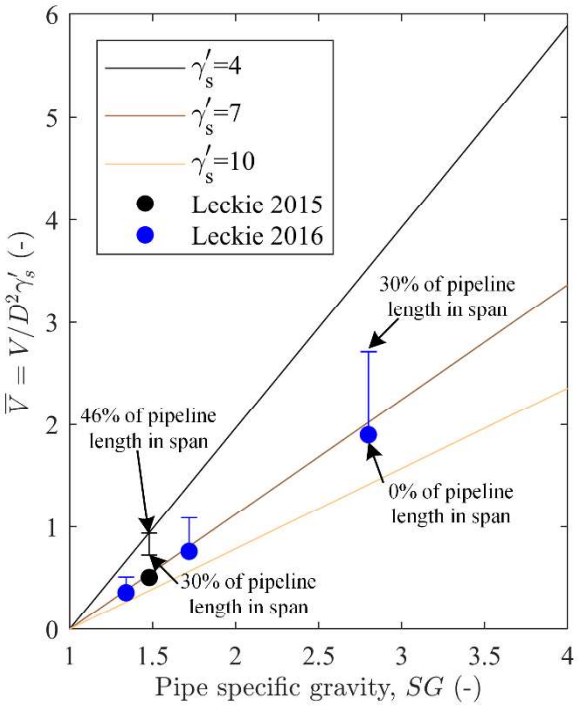

Figure 3. Relationship between pipeline SG and $\bar{V} = V/D^2\gamma'_s$. Solid lines indicate baseline V. Solid circles indicate baseline values for example pipelines with no spanning and error bars correspond to inferred range of $\bar{V}$ due to spanning proportions.

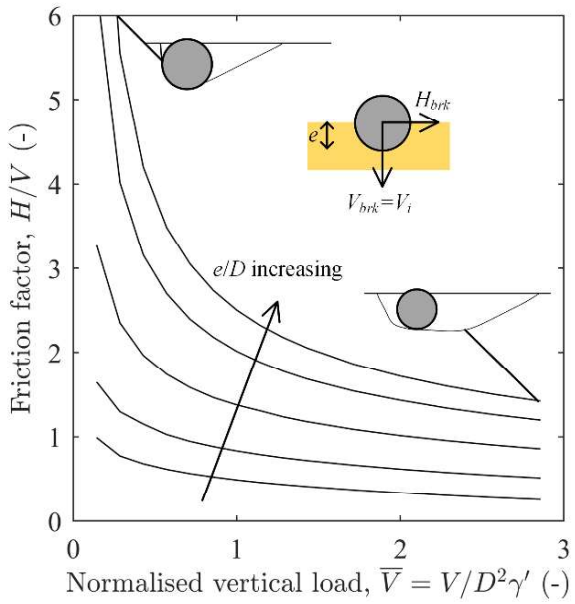

Figure 4. Flat seabed: effect of embedment. e/D increasing over 0.1, 0.25, 0.5, 0.75 and 0.9. Schematics show example mobilized soil volume at failure for $\bar{V}$=0.14 and 2.9; e/D=0.9.

Figure 4 shows the variation in normalised breakout resistance (so-called 'friction factor' – H/V) for a flat seabed, as it varies with applied vertical load as a function of local embedment. The H/V resistance ratio generally increases with embedment, but the relationship describing this increase depends on $\bar{V}$ varying from approximately linear at larger $\bar{V}$~3 to being proportional to embedment to a power of ~2.3 for $\bar{V} = 0.14$. For a single embedment, H/V reduces with increasing $\bar{V}$ due to combined loading effects, although the magnitude of horizontal resistance increases over this vertical load range. The nonlinearity

of H/V reduction occurs because the failure mechanism transitions to a more predominantly vertical bearing failure rather than a pure sliding failure, the latter of which is more analogous to a retaining wall.

Select H/V results for $e/D = 0.1$ and 0.9 are reproduced on Figures 5 and 6 along with equivalent results for $\pm 20°$ seabed slopes away from the pipeline. Overlain on these are predictions based on two modifications of a simple approach for resistance to allow for the effect of a sloping seabed. The simple approach combines terms for friction beneath the pipe and passive resistance linked to embedment. The original form was suggested by Zhang et al. (2002):

$$H = \mu_0 V + \frac{1}{2}\gamma_s' e^2 \left(K_p - K_a\right) \tag{2}$$

where μ_0 is a friction coefficient ($\tan(\phi)$), e is the dimensional local pipeline embedment, and K_p and K_a are passive and active earth pressure coefficients:

$$K_p = \frac{1 + \sin\theta}{1 - \sin\theta} \tag{3a}$$

$$K_a = \frac{1 - \sin\theta}{1 + \sin\theta} \tag{3b}$$

On Figures 5 and 6, Eq. 2 is modified to allow for seabed slope using two different approaches:

(a) Slope-modified friction: the first term is modified following Wilkinson et al. (1988) – Figure 5:

$$H = \frac{\mu_0 + \tan\theta}{1 - \mu_0 \tan\theta} V + \frac{1}{2}\gamma_s' e^2 \left(K_p - K_a\right) \tag{4}$$

(b) Passive-modified friction: the second term is adjusted with varying values of K_p and K_a to account for the change in passive resistance due to sloping backfill – Figure 6. For (b), a secondary set of OptumG2 analyses were conducted to determine the variation in K_p and K_a, for a retaining wall with a purely horizontal driving or resisting force. A reasonable fit to these results is:

$$K_p^* = K_p \left(1 + 2\left(\frac{\tan(\theta)}{1 - \tan(\theta)}\right)\right) \tag{5a}$$

$$K_a^* = K_a \left(1 + 0.5\left(\frac{\tan(\theta)}{1 - \tan(\theta)}\right)\right) \tag{5b}$$

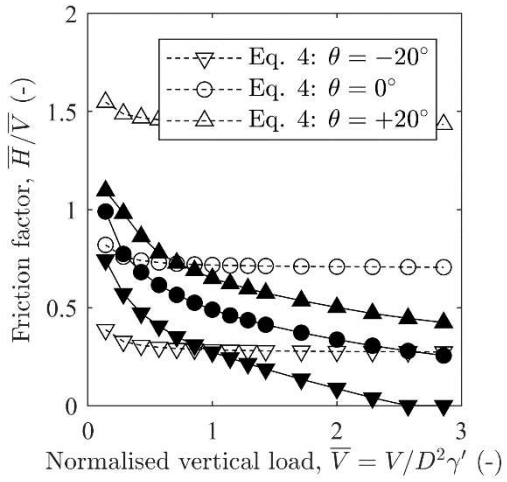

(a) Shallow: *e/D*=0.1

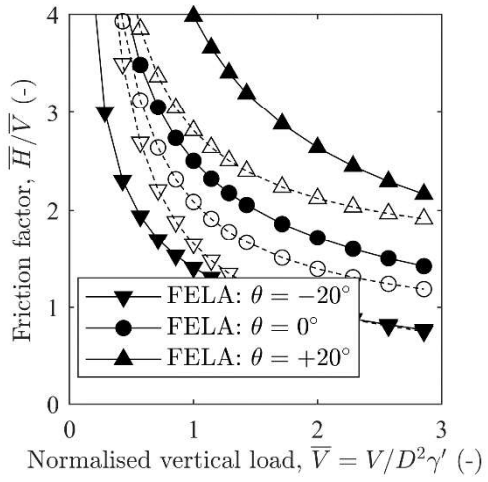

(b) Deep: *e/D*=0.9

Figure 5. Effect of seabed slope for *e/D* = 0.1 and 0.9. Comparison with Eq. 3 (slope-modified friction term). Note split legend.

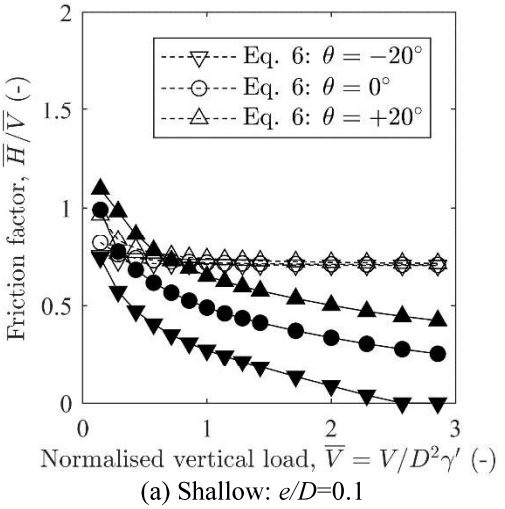

(a) Shallow: *e/D*=0.1

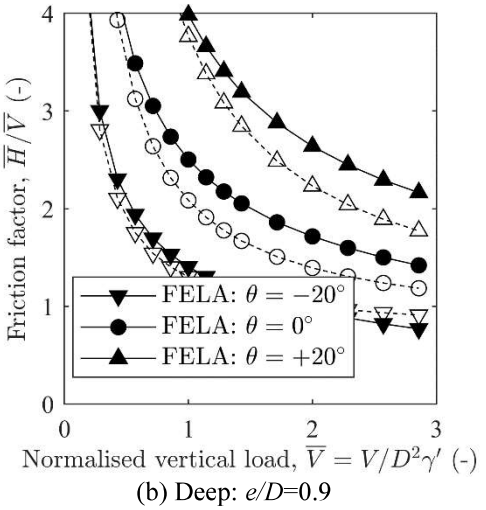

(b) Deep: *e/D*=0.9

Figure 6. Effect of seabed slope for *e/D* = 0.1 and 0.9. Comparison with Eq. 4-5 (slope-modified passive term). Note split legend.

Implementing these results into Eq. 2:

$$H = \mu_0 V + \frac{1}{2}\gamma_s' e^2 \left(K_p^* - K_a^*\right) \quad (6)$$

Figure 5 and 6 compare these simple calculation models with the limit analysis results.

For $e/D = 0.1$, the limiting friction reduces significantly as pipe weight increases (Fig 5a). The estimate based on Eq. 4 for no slope, i.e. θ = 0 is a 20% underprediction at very low values of $\bar{V}$ and overpredicts the resistance for all $\bar{V} > 1$. The effect of seabed slope is over-predicted by the slope-modified friction method (Eq. 4), and this method generally over-predicts the friction for higher $\bar{V}$. Conversely, the slope-modified passive resistance approach (Eq. 6) shows almost no effect of slope at small embedment because the passive component is small (Fig. 6a). Neither method appears to work well at small e/D.

By contrast, for large local embedment (e/D = 0.9), the slope-modified friction approach (Eq. 4) generally agrees to within 30% of the limit analysis results for $\bar{V} > 1$ and captures the general effect of seabed slope (Fig. 5b). However, the slope-modified passive approach (Eq. 6; Fig. 6b) provides better prediction of the overall resistance across the $\bar{V}$ range and for both extremes of seabed slope.

These comparisons are further illustrated on Figure 7 and 8, which shows the ratio of horizontal resistance with slope angles of -20° and 20°, and compared with the ratios predicted by Eq. 4 and 6, respectively. Considering the limit analysis results, the changes in resistance due to sloping seabed are most sensitive to the magnitude of $\bar{V}$ at small local embedment. This occurs because for small local embedments the failure mechanism is more localised and changes as a stronger function of vertical load. Since changes in the applied vertical load cause proportionally larger changes in the volume of soil mobilised during failure (e.g. Figure 9c and 9d), the slope has an strong effect on the response at higher vertical loads (i.e. relatively more soil is 'lifted' up the slope or 'pushed' down the slope).

Conversely, for larger local embedments with an upwards adjacent slope ($\theta > 0$), increasing $\bar{V}$ reduces the influence of the slope. This occurs because the shape of the failure mechanism (i.e. the angles of the mechanism relative to horizontal) at large embedments changes more for low vertical loads than high. These differences are evident comparing Figure 9b and 9d where there is a more significant change in the component (and trajectory) of soil lifted vertically for $\bar{V} = 0.14$ than for $\bar{V} = 2.9$. However, with negative slope angles and large local embedment, the volume of soil mobilised increases with vertical load for both the flat seabed and downward sloping cases; but no significant further work is done against gravity since the trajectory of the lifted soil volumes does not change significantly with increasing $\bar{V}$.

Figures 10 shows example results demonstrating the relative changes in horizontal capacity for different slope angles, as a function of local embedment. The analysis results were fitted with linear trend lines with an intercept value of 1 at $\theta = 0°$. Predictions based on Eq. 6 are compared and as before, there is reasonable comparison in terms of the general trends but not the magnitude of the errors. This reiterates the discrepancies shown on Figure 8. Although the magnitude of the predictions by Eq. 6 can sometimes vary from the analyses, the trends of the results (i.e. the ratios increasing with embedment) are consistent. The comparison suggests that Eq. 6 provides the better approach for an estimate of the variation in $\bar{H}$ with sloping seabed profiles; but case specific analyses should be conducted in practice.

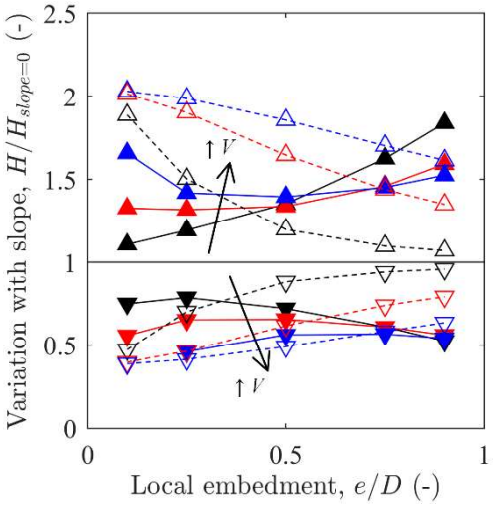

Figure 7. Variation in capacity for -20° and 20° seabed slope as a function of vertical load and local embedment. $\bar{V}$ = 0.14, 1.0 and 2.9. Solid lines and symbols – current study, FELA. Dashed lines and open symbols – relative difference as per Eq. 4.

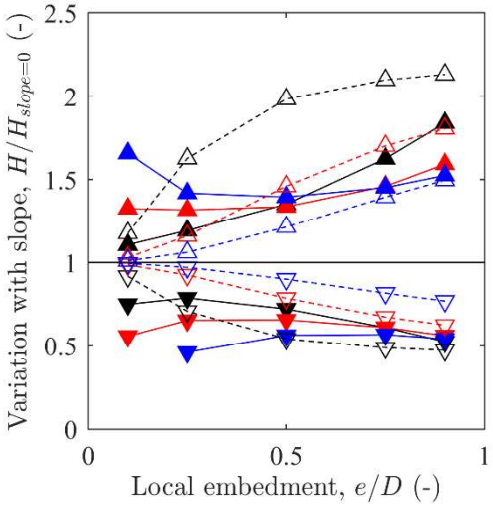

Figure 8. Variation in capacity for -20° and 20° seabed slope as a function of vertical load and local embedment. $\bar{V}$ = 0.14, 1.0 and 2.9. Solid lines and symbols – current study, FELA. Dashed lines and open symbols – relative difference as per Eq. 6.

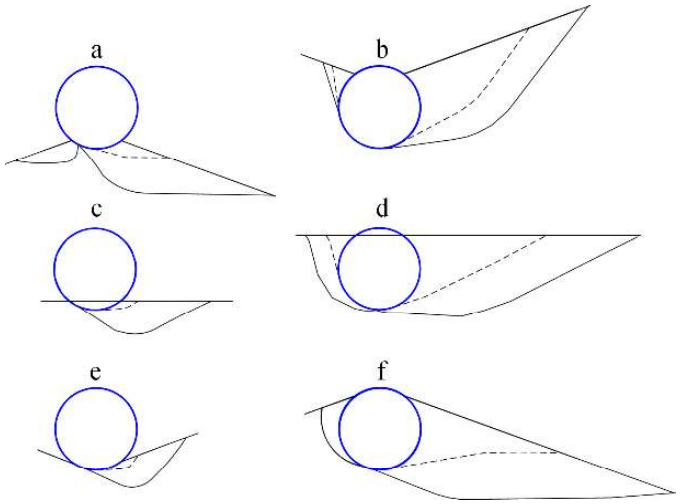

Figure 9. Example failure mechanisms illustrated by volume of mobilized soil displacements. Dashed lines - $\bar{V} = 0.14$. Solid lines - $\bar{V} = 2.9$

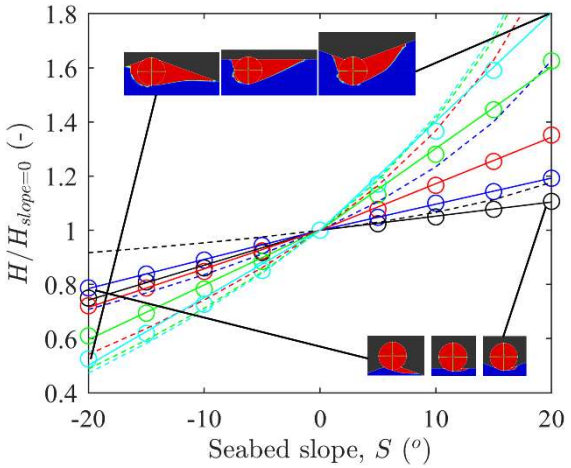

Figure 10. Variation in capacity with seabed slope and embedment - $\bar{V} = 0.14$. Black – e/D=0.1. Blue – e/D=0.25. Red – e/D=0.5. Green – e/D=0.75. Cyan – e/D=0.9. Dash lines - Eq. 5.

4 CONCLUSIONS

The foregoing results illustrate that the horizontal pipeline resistance in 2D cases is sensitive to both the local embedment, e/D, and the adjacent seabed slope, θ, in addition to $\bar{V}$. The analyses in this paper covered a range of these characteristics across a large parameter space covering many practical scenarios ($e/D = [0.1, 0.9]$, $\theta = [-20°, 20°]$ and $\bar{V} < 3$). Over this space, the vertical load level has a clear and strong influence on the available equivalent friction. However, the local embedment is shown to be particularly important at small values of $\bar{V}$; and the influence of seabed slope is dominant (with an effect of similar order to $\bar{V}$) at large local embedments.

The results indicate that a modification of the commonly used approach to predict pipeline breakout resistance comprising friction on the pipe plus a slope-adjusted passive resistance term can provide reasonable estimates (Eq. 6). The comparison is generally best for large e/D where the failure mechanism is most similar to a retaining wall.

REFERENCES

Bransby, M.F., Borges Rodriguez, A., Zhou, H., Low, H.E. & White, D.J. (2014). Sediment mobility effects on seabed resistance for unburied pipelines. Proc. Offshore Tech. Conf.

Chatterjee S., White D.J. & Randolph M.F. (2013). Coupled consolidation analysis of pipe-soil interactions. Canadian Geotechnical Journal, 50(6): 609-619

Cornett, A., Baker, S., Riedel, P., & Knox, P. (2015). Optimization of Rock Berms for Pipeline Stabilization Subject to Intense Hydrodynamic Forcing. Proc. 34th International Conference on Ocean, Offshore and Arctic Engineering

Davis, E. (1968). Theories of plasticity and failures of soil masses. In Soil mechanics, selected topics.

Draper S., Griffiths T., Cheng L., White D.J. & An. H. 2018. Modelling changes to submarine pipeline embedment and stability due to pipeline scour. Proc. Conf. on Ocean, Offshore & Arctic Engineering, Madrid, Spain. Paper OMAE2018-77985.

Gourvenec S.M. & White D.J. 2010. Elastic solutions for consolidation around seabed pipelines. Proc. Offshore Technology Conference, Houston. Paper 20554

Griffiths, T., Shen, W., Xu, M., & Leggoe, J. (2012). Comparison of recent parametric trenched and partially embedded/spanning pipelines with DNV-RP-F109 load reduction design curves. In ASME 2012 31st International Conference on Ocean, Offshore and Arctic Engineering (pp. 207-224). American Society of Mechanical Engineers.

Griffiths T., Draper S., White D.J., Cheng L., An. H. & Fogliani A. 2018. Improved stability design of subsea pipelines on mobile seabeds: Learnings from the STABLEpipe JIP. Proc. Conf. on Ocean, Offshore & Arctic Engineering, Madrid, Spain. Paper OMAE2018-77217

Leckie S., Draper S., White D.J., Cheng L., Griffiths T. & Fogliani A. 2018. Observed changes to the stability of a seabed pipeline caused by seabed mobility. Ocean Engineering 169:159-176

Leckie S., Mohr H., Draper S., McLean D., White D.J. & Cheng L. 2016. Sedimentation-induced burial of subsea pipelines: observations from field data and laboratory experiments. Coastal Engineering 114:137-158

Leckie, S., Draper, S., White, D.J., Cheng, L. & Fogliani N. 2015. Lifelong embedment and spanning of a pipeline on a mobile seabed. Coastal Engineering. 95:130-146.

Martin C.M. & White D.J. 2012. Limit analysis of the undrained capacity of offshore pipelines. Géotechnique, 62(9):847-863

OptumCE (2018). OptumG2, http://optumce.com/.

Tom, J.G., Leckie S.H.F., White D.J. & Draper, S. 2015. Drained breakout resistance of a pipeline on a mobile seabed. Proc. Int. Conf. Offshore Mech. and Arctic Engng. OMAE2015-41206

Tom J.G., Draper S.D., White D.J. & O'Neill M.P. 2016. Risk-based assessment of scour around subsea infrastructure. Proc. Offshore Technology Conference, Houston OTC27131

Tom J.G. & White D.J. 2019. Drained bearing capacity of shallowly-embedded pipelines. ASCE J. Geotechnical and Geoenvironmental Engineering. *Accepted pending revisions.*

Tong, F., & Cheng, L. (2016). Numerical Study on Steady Flow around a Pipeline Laid on Seabed with Gaps. In The Twelfth ISOPE Pacific/Asia Offshore Mechanics Symposium. International Society of Offshore and Polar Engineers.

Verley, R. L. P., & Sotberg, T. (1994). A soil resistance model for pipelines placed on sandy soils. Journal of Offshore Mechanics and Arctic Engineering, 116(3), 145-153.

Westgate Z.J., Haneberg, W. & White D.J. 2016. Modelling the spatial variability in as-laid embedment for HPHT pipeline design. Canadian Geotechnical Journal. 53(11): 1853-1865.